Physica B 600 (2021) 412579

Contents lists available at ScienceDirect

Physica B: Physics of Condensed Matter

journal homepage: http://www.elsevier.com/locate/physb

Comparison of the effects of Sr^{2+} and Ca^{2+} substitution on the structural and electronic properties of the perovskites $CH_3NH_3Pb_{1-x}Y_xI_3$ (Y=Sr, Ca) by using the Density Functional Theory

C. Soykan [a,*], H. Gocmez [b]

[a] Vocational School of Health Services, Ahi Evran University, Kırşehir, Turkey
[b] Department of Metallurgy and Materials Engineering, Dumlupınar University, Kütahya, Turkey

ARTICLE INFO

Keywords:
Heterovalent perovskite CH3NH3Pb(1-x)Y(x)I3 (Y=Sr,Ca)
Density Functional Theory
Electronic properties
Photovoltaic
Substitution

ABSTRACT

The Vienna ab-initio simulation package (VASP) and Density Functional Theory (DFT) calculation method are used to study the structural and detailed electronic properties through atomic substitution in the $CH_3NH_3Pb_{(1-x)}Y_{(x)}I_3$ (Y=Sr, Ca x = 0.125, 0.25, 0.50, 0.75, and 1.0) perovskites. We determined that the non-stoichiometric crystal structures were calculated as a distorted orthorhombic phase as predicted by the tolerance factor range $0.7 < t < 0.9$. The bandgaps of the stoichiometric $CH_3NH_3SrI_3$ and $CH_3NH_3CaI_3$ compounds are calculated 3.261 eV (Q → Γ indirect) and 3.144 eV (Q → Γ indirect), respectively and they are very high for ideal photo absorbers. We were determined that the bandgap (Γ → Γ direct) of the $CH_3NH_3Pb_{0.875}Ca_{0.125}I_3$, $CH_3NH_3Pb_{0.750}Ca_{0.250}I_3$, and $CH_3NH_3Pb_{0.875}Sr_{0.125}I_3$ compounds are calculated 1.44 eV, 1.54 eV, and 1.525 eV respectively and are more suitable for ideal photo absorbers. It was seen that Ca^{2+} substitution was more successful than Sr^{2+} substitution.

1. Introduction

Recently, perovskite compounds have attracted a lot of attention due to their high power conversion efficiencies, low fabrication costs, superconductivity, electronic, and optical properties. Organic-inorganic hybrid perovskite compounds have occurred ABX_3form, in which $A = [CH_3NH_3]^+$ cation, $B = Pb^{2+}$ cation, and $X = I^-$ anion [1]. There are many studies in which anions such as CI^- and Br^- are substituted instead of the $X = I^-$ anion [2–8]. Also, the electronic and optical properties of perovskite compounds in ABX_3 form was studied by substituting inorganic cations such as Pd^{2+}, Ge^{2+}, Sn^{2+}, Sr^{2+}, Ca^{2+} and Ag^+ instead of the $B = Pb^{2+}$ cation [9–19]. Moreover, in our previous study, the change in the structural and electronic properties of the $CH_3NH_3Pb_{(1-x)}Bi_{(x)}I_3$ (x = 0.125, 0.250, 0.500, 0.750, 1.000) perovskite compound by the substitution of Bi instead of Pb cation has investigated as systematically [20].

There are many studies on structural parameters of $CH_3NH_3PbI_3$ perovskite compounds such as lattice constants and crystal symmetries [5,6,17,19–25]. Moreover, there are studies on the electronic properties of bandgap and direct-indirect band transitions for $CH_3NH_3PbI_3$ perovskite crystals [6,13–15,17–23,26–31]. Since this study was built on the substitution of Sr^{2+} and Ca^{2+} cations instead of the Pb^{2+} cation in $CH_3NH_3PbI_3$ perovskite compounds, the previous experimental and theoretical studies have been limited to studies on Sr^{2+} and Ca^{2+} substitution. The bandgap of $CH_3NH_3SrI_3$ was calculated to be 3.6 eV using density functional theory (DFT) calculations by Jacobsson and et al. [18]. The Jacobsson study showed that although the Sr^{2+} ions have almost the same ionic radius as Pb^{2+}, the calculated bandgap (as 3.6 eV) of the $CH_3NH_3SrI_3$ crystal structure is not suitable for an effective photo absorber [18]. Besides, the lattice constants of $CH_3NH_3CaI_3$ perovskite compound were investigated using first-principles calculations based on DFT by Uribe and et al. [19]. In the study of Uribe, the bandgap of $CH_3NH_3CaI_3$ perovskite compound was calculated as 3.40 eV in the R→Γ direction (as indirect band transition) [19]. Moreover, except for the above, to the best of our knowledge, no detailed theoretical and experimental data concerning the structural and bandgap properties of the $CH_3NH_3CaI_3$ and $CH_3NH_3SrI_3$ perovskite compounds. Farther, when Pb^{2+} is removed from the $CH_3NH_3PbI_3$ compound and replaced with an ion such as Sr^{2+} or Ca^{2+}, it was seen that the bandgap of the obtained crystal structure is very high for ideal photo absorbers. One of the best approaches that can be proposed for the solution of this high bandgap problem may be the creation of the non-stoichiometric $CH_3NH_3Pb_{(1-x)}Y_{(x)}I_3$ (Y=Sr, Ca, x = 0.125, 0.250, 0.500, 0.750)

* Corresponding author.
E-mail address: cengiz.soykan@ahievran.edu.tr (C. Soykan).

https://doi.org/10.1016/j.physb.2020.412579
Received 19 March 2020; Received in revised form 1 September 2020; Accepted 13 September 2020
Available online 19 September 2020
0921-4526/

compound forms, as in our study.

Our main aim is to form the non-stoichiometric $CH_3NH_3Pb_{(1-x)}Y_{(x)}I_3$ (Y=Sr, Ca, x = 0.125, 0.250, 0.500, 0.750) compounds formed by substituted Sr^{2+} and Ca^{2+} ions instead of Pb^{2+} according to Goldschmidt's empirical substitution rules, and it is to reduce the bandgap of $CH_3NH_3Pb_{(1-x)}Y_{(x)}I_3$ (Y=Sr, Ca) solar cell material to an appropriate value for the ideal photo absorbers specified in the Shockley Queisser (SQ) limit [32]. Because the bandgaps of $CH_3NH_3PbI_3$, $CH_3NH_3SrI_3$, and $CH_3NH_3CaI_3$ phases have been reported to be too high for ideal photo absorbers. Moreover, it is built on comparing the effects of Sr^{2+} and Ca^{2+} substitution on the structural and electronic properties of the perovskites $CH_3NH_3Pb_{(1-x)}Y_{(x)}I_3$ (Y=Sr, Ca) and determining the most efficient bandgap according to the SQ limit.

2. Computational method

Ab-*initio* total-energy calculations based on the Density Functional Theory (DFT) were performed by using the Vienna ab-*initio* simulation package (VASP) with the Generalized Gradient Approximation (GGA) developed by Burke, Perdew, and Ernzerhof [33–41]. In this study, the Projector Augmented Wave (PAW) method, a modern version of the Augmented Plane Wave (APW) method, was used. The PAW method was developed by Blöchl to accurately and efficiently calculate the electronic structure of materials [42]. It is based on the DFT. It contains the numerical advantages of pseudopotential calculations. In the self-consistent iterations, ıt consider both the correct nodal behavior of the valence-electron wave functions and including upper core states in addition to valance states. Thus preserves the physics of all-electron calculations.

While the kinetic energy cutoff values were determined to be 600 eV for stoichiometric phases ($CH_3NH_3PbI_3$, $CH_3NH_3SrI_3$, and $CH_3NH_3CaI_3$), were determined to be 500 eV for non-stoichiometric phases ($CH_3NH_3Pb_{(1-x)}Y_{(x)}I_3$ (Y=Sr, Ca, x = 0.125, 0.250, 0.500, 0.750)). The energy convergence criterion of the electronic self-consistency was fixed as 10^{-8} eV/atom for all crystal phases. The Brillouin zone integrations were carried out by Monkhorst-Pack special points mesh with a grid size of 12x12x12 for stoichiometric phases ($CH_3NH_3PbI_3$, $CH_3NH_3SrI_3$, and $CH_3NH_3CaI_3$), and 6 × 6 × 6 for non-stoichiometric phases ($CH_3NH_3Pb_{(1-x)}Y_{(x)}I_3$ (Y=Sr, Ca, x = 0.125, 0.250, 0.500, 0.750)) [43]. The valance electron configurations C, N, H, Pb, Sr, Ca, and I atoms are $2s^22p^2$, $2s^22p^3$, $1s^1$, $5d^{10}6s^2$ $6p^2$, $4s^24p^65s^2$, $3s^23p^64s^2$, and $5s^2$ $5p^5$, respectively.

Firstly, the geometric optimizations were performed for the stoichiometric $CH_3NH_3PbI_3$, $CH_3NH_3SrI_3$, and $CH_3NH_3CaI_3$ phases. Secondly, the supercell crystal structures were constructed with a 2 × 2 × 2 ratio iteration by using the optimized cubic $CH_3NH_3PbI_3$ crystal structure (as calculated in our previous study $a = 6.406$ Å) [20]. Thirdly, Sr^{2+} ve Ca^{2+} ions are substituted instead of Pb^{2+} in the supercell crystal phases by considered Goldshmidt's empirical substitution rules. In addition, the non-stoichiometric ratios (x = 0.125, 0.250, 0.500, and 0.750) were considered in the this process. A look at the periodic table can be seen as a number of candidates Calcium (Ca) and Strontium (Sr), where Ca has a slightly smaller ionic radius (Ca^{2+} = 114 pm) and Sr has almost the same ionic radius as Pb (Sr^{2+} = 132 pm, Pb^{2+} = 133 pm). Thus, the difference between Pb^{2+} and Ca^{2+} ionic radius was calculated as 13.63%. The empirical rules for element substitution to Goldschmidt, if the ionic radius differs by less than 15%, a full perfectly substitution can occur, but, if the size differs between 15% and 30%, limited substitution can occur [44]. Hence the Sr^{2+} ve Ca^{2+} ions are substituted instead of Pb^{2+} are full perfectly substitution, because the ionic radius differs by less than 15%. Besides, the Goldschmidt tolerance factor (*t*) was calculated as t = 0.8075 and 0.8529 for the Sr^{2+} ve Ca^{2+} substitutions respectively. The calculated tolerance factor *t* is determined at $0.7 < t < 0.9$ [45–47]. Thus, our studied crystal structures are expected to be in tetragonal, orthorhombic, or rhombohedral form. All details of the tolerance factor (*t*) calculations are presented in our previous study [20]. Using all the above-mentioned approaches, structural (lattice constants and crystal forms) and electronic (DOS, pDOS, and Bandgap) properties were investigated to systematically analyze the effect of Sr^{2+} and Ca^{2+} substitution on the structural and electronic nature of the perovskite ($CH_3NH_3Pb_{(1-x)}Y_{(x)}I_3$ (Y=Sr, Ca, x = 0.125, 0.250, 0.500, 0.750, 1.000)) crystal structures.

3. Results and discussion

3.1. Structural properties of stoichiometric phases

In this study, the structural properties of $CH_3NH_3PbI_3$ perovskite cubic structure were recalculated for comparison with the previous result [20]. The new results were seen to be compatible with the previous study [20]. Moreover, the non-stoichiometric $CH_3NH_3SrI_3$ and $CH_3NH_3CaI_3$ phases are constructed by substitution Sr^{2+} and Ca^{2+} ions instead of Pb^{2+} ion. The crystal structures of stoichiometric $CH_3NH_3PbI_3$, $CH_3NH_3SrI_3$, and $CH_3NH_3CaI_3$ are given in Fig. 1a) and b) (unit cell with 12 atoms). In our calculations, the lattice constant of the cubic phase of $CH_3NH_3PbI_3$ was calculated as 6.406 A^0 with a unit cell volume of 262.88 A^3. The calculated lattice constant is consistent with the theoretical data in the range of from 6.172 A^0 to 6.420 A^0 [6,17,19, 21–23] and also the experimental lattice constants varying between 6.180 $A^0$and 6.288 A^0 [5,24,25]. The lattice constant calculated as 6.406 A^0 differs 2–3% ratio deviation from the experimental data.

The calculated tolerance factor *t* is determined at $0.7 < t < 0.9$ for substitution Sr^{2+} and Ca^{2+} instead of Pb^{2+} ion [45–47]. All details of the tolerance factor (*t*) calculations are presented in our previous study [20]. Thus, our studied crystal structures are expected to be in tetragonal, orthorhombic, or rhombohedral form. The lattice constants of stoichiometric $CH_3NH_3SrI_3$ phase are also calculated as 6.759 A^0, 6.527 A^0 and 6.542 A^0. The crystal structure of the stoichiometric $CH_3NH_3SrI_3$ phase has been determined as a distorted orthorhombic structure. The best of our knowledge, no detailed theoretical or experimental data concerning stoichiometric $CH_3NH_3SrI_3$ structural properties have been reported in the literature. Moreover, the structural properties of stoichiometric $CH_3NH_3CaI_3$ phase are determined as 6.503 A^0, 6.133 A^0 and 6.145 A^0. This crystal structure is also a distorted orthorhombic structure. These results are consistent with the estimates of the calculated tolerance factor (*t*). There is a theoretical study concerning with the distorted orthorhombic structure of stoichiometric $CH_3NH_3CaI_3$ calculated by Uribe et al. [19]. Our results are deviated by 2–3% from Uribe's structural results. However, there are no other experimental or theoretical studies we can compare. Our results are presented in Table 1 for comparison with other experimental and theoretical studies.

3.2. Structural properties of non-stoichiometric phases

The crystal structure of $CH_3NH_3PbI_3$ given in Fig. 1a) was selected as the initial phase and x = 0.125 was taken to form the first non-stoichiometric $CH_3NH_3Pb_{(1-x)}Y_{(x)}I_3$ (Y=Sr, Ca, x = 0.125) structure. The crystal lattice was shifted to 2 × 2 × 2 (containing C 8, N 8, H 48, Pb 7, Sr or Ca 1 and I 24 atoms) have been obtained the $CH_3NH_3Pb_{0.875}Y_{0.125}I_3$ supercell. This supercell is given in Fig. 2 a). Similarly, x = 0.25, 0.50 and 0.75 (Y=Ca, Sr) were selected to obtain $CH_3NH_3Pb_{0.750}Y_{0.250}I_3$, $CH_3NH_3Pb_{0.500}Y_{0.500}I_3$ and $CH_3NH_3Pb_{0.250}Y_{0.750}I_3$, respectively. Supercells of these phases are presented in Fig. 2b) and c) and d), respectively. Also, the substitution situations of Ca^{2+} and Sr^{2+} ions in the nearest neighbors are shown in Fig. 2 c1), and the substitution situations in the second nearest neighbors in Fig. 2 c2).

All non-stoichiometric substituted $CH_3NH_3Pb_{(1-x)}Y_{(x)}I_3$ (Y=Sr, Ca x = 0.125, 0.25, 0.50 and 0.75) crystal structures were calculated as a distorted orthorhombic phase as predicted by the tolerance factor range $0.7 < t < 0.9$. It is seen that the crystal structures of the non-stoichiometric phases are transformed from the cubic phase to a

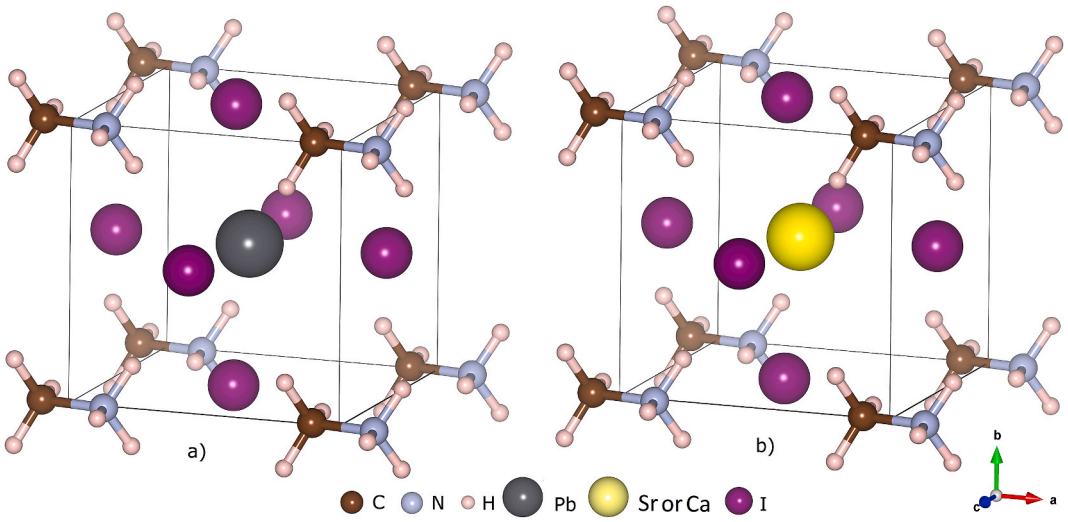

Fig. 1. a) $CH_3NH_3PbI_3$ and b) $CH_3NH_3SrI_3$ and $CH_3NH_3CaI_3$ perovskite cubic and orthorhombic phases unit cell crystal structures. Brown, gray, cream, black, yellow, and purple circles in the pictures represent C, N, H, Pb, Sr or Ca and I atoms, respectively. (For interpretation of the references to colour in this figure legend, the reader is referred to the Web version of this article.)

Table 1
The lattice constants of the stoichiometric $CH_3NH_3PbI_3$, $CH_3NH_3SrI_3$, and $CH_3NH_3CaI_3$ crystal structures and the other theoretical and experimental data.

Structure	Method	Lattice Constants (A^0)			Ref.
		a	*b*	*c*	
$CH_3NH_3PbI_3$	our cal.	6.406	6.406	6.406	
	other cal.	6.330	6.330	6.330	[6]
		6.340	6.370	6.350	[17]
		6.219	6.184	6.251	[19]
		6.406	6.406	6.406	[20]
		6.420	6.420	6.420	[21]
		6.310	6.310	6.320	[22]
		6.172	6.149	6.218	[23]
	exp.	6.180	6.180	6.180	[5]
		6.328	6.328	6.328	[24]
		6.288	6.288	6.288	[25]
$CH_3NH_3SrI_3$	our cal.	6.759	6.527	6.542	
$CH_3NH_3CaI_3$	our cal.	6.503	6.133	6.145	
	other cal.	6.263	6.278	6.369	[19]

distorted orthorhombic phase, while the deviation rates in the lattice constants are very small. The calculated structural properties of non-stoichiometric phases are listed in Table 2. Also, the effect of Ca^{2+} and Sr^{2+} ions on the structural and electronic state of the material when substituted in the second nearest neighbor position for x = 0.50 was studied in Fig. 2 c2. In this substitution state, the lattice constants calculated for the $CH_3NH_3Pb_{0.50}Y_{0.50}I_3$ (Y═Ca x = 0.50) structure are a = 12.629 A^0, b = 12.599 A^0, and c = 12.820 A^0. Similarly, within the structure of the $CH_3NH_3Pb_{0.50}Y_{0.50}I_3$ (Y═Sr x = 0.50), a = 12.871 A^0, b = 12.830 A^0 and c = 13.093 A^0. The atomic positions of Ca^{2+} and Sr^{2+} ions in the second near neighbor state are calculated as (0.73008 for Ca^{2+}, 0.24996 for Ca^{2+}, 0.74289 for Ca^{2+}; 0.23002 for Ca^{2+}, 0.24996 for Ca^{2+}, 0.24339 for Ca^{2+}; 0.23001 for Ca^{2+}, 0.74996 for Ca^{2+}, 0.24339 for Ca^{2+}; 0.73007 for Ca^{2+}, 0.74996 for Ca^{2+}, 0.74288 for Ca^{2+}; 0.72669 for Sr^{2+}, 0.24997 for Sr^{2+}, 0.74066 for Sr^{2+}; 0.22645 for Sr^{2+}, 0.24999 for Sr^{2+}, 0.24023 for Sr^{2+}; 0.72669 for Sr^{2+}, 0.74997 for Sr^{2+}, 0.74066 for Sr^{2+}; 0.22645 for Sr^{2+}, 0.74999 for Sr^{2+}, 0.24023 for Sr^{2+}), respectively. It is determined that the difference between lattice constants is quite small (x:0.024%, y:0.04%, and z:0.20% for Ca^{2+}; x:0.031%, y:0.14%, and z:0.20% for Sr^{2+}, respectively). The results are highly consistent with the lattice constants obtained for the nearest neighbor position when compared with Table 2. At the same time, the lattice angles are also very compatible. The space symmetry of crystal structures does not change either. Therefore, there is no significant structural change in the crystal structure due to between Ca^{2+} and S^{2+} ions settling in the nearest neighbor position or the second nearest neighbor position. In addition, the Structural properties of non-stoichiometric $CH_3NH_3Pb_{(1-x)}Y_{(x)}I_3$ (Y═Sr, Ca) perovskite crystal phases are substituted by both Sr^{2+} and Ca^{2+} at x (0.125, 0.250, 0.500, and 0.750) ratios are given for the first time in this study.

3.3. Electronic properties of stoichiometric phases

For the perovskite structures in the $A-B-X_3$ general form, the electronegativity of the B cation was reported to be more effective on the bandgap than the A cation [48,49]. Accordingly, reducing the electronegativity of B cation will increase the bandgap of the material. Also, the character of the $B-X$ bond is effective on bandgap and the increase in the antibonding character of the $B-X$ bond will also increase bandgap [48]. Differences in orbit symmetries are a source of these effects and can lead to the possibility of different hybridizations. Moreover, in order words, Since Pb^{2+}, Sr^{2+}, and Ca^{2+} cations lose electrons, the electrostatic attraction between the nucleus and the remaining electrons increases. Accordingly, the electrons are drawn more towards the center, and the cation's radius becomes smaller. Thus, the electrostatic charge of the ionic bond envelops all the walls of the ion. As a result, the cation in the bond tends to be surrounded by the highest number of anions. With this effect, since the energies of $B-X$ bonds will increase, $B-X$ bonds will be even stronger. Thus, the bandgap of the material will be reduced. The value of the bandgap is very important for an ideal photo absorber. It has been reported by Shockley and Queisser that the bandgap around 1.5 eV would be ideal (SQ limit) [32].

Firstly, the bandgap and type of band transitions (direct and indirect) were calculated for stoichiometric perovskite $CH_3NH_3PbI_3$, $CH_3NH_3SrI_3$, and $CH_3NH_3CaI_3$ crystal structures are given in Table 3. As seen in Table 3, the $CH_3NH_3PbI_3$ structure is highly compatible with both experimental and theoretical studies [6,13–15,17–23,26]. However, the calculated bandgap (1.682 eV, $R \rightarrow R$ direct) is slightly high for an ideal photo absorber. The bandgaps given in Refs. [15,31] are optical and have been added to Table 3 because they are compatible with other studies. Our aim is not to compare the optical band gap with the electronic bandgap. In our study, we do not claim that the optical band gap matches the electronic bandgap. When Sr^{2+} and Ca^{2+} ions are substituted instead of Pb^{2+} to both reduce the value of the bandgap and reduce the toxic Pb concentration, the bandgaps are calculated for

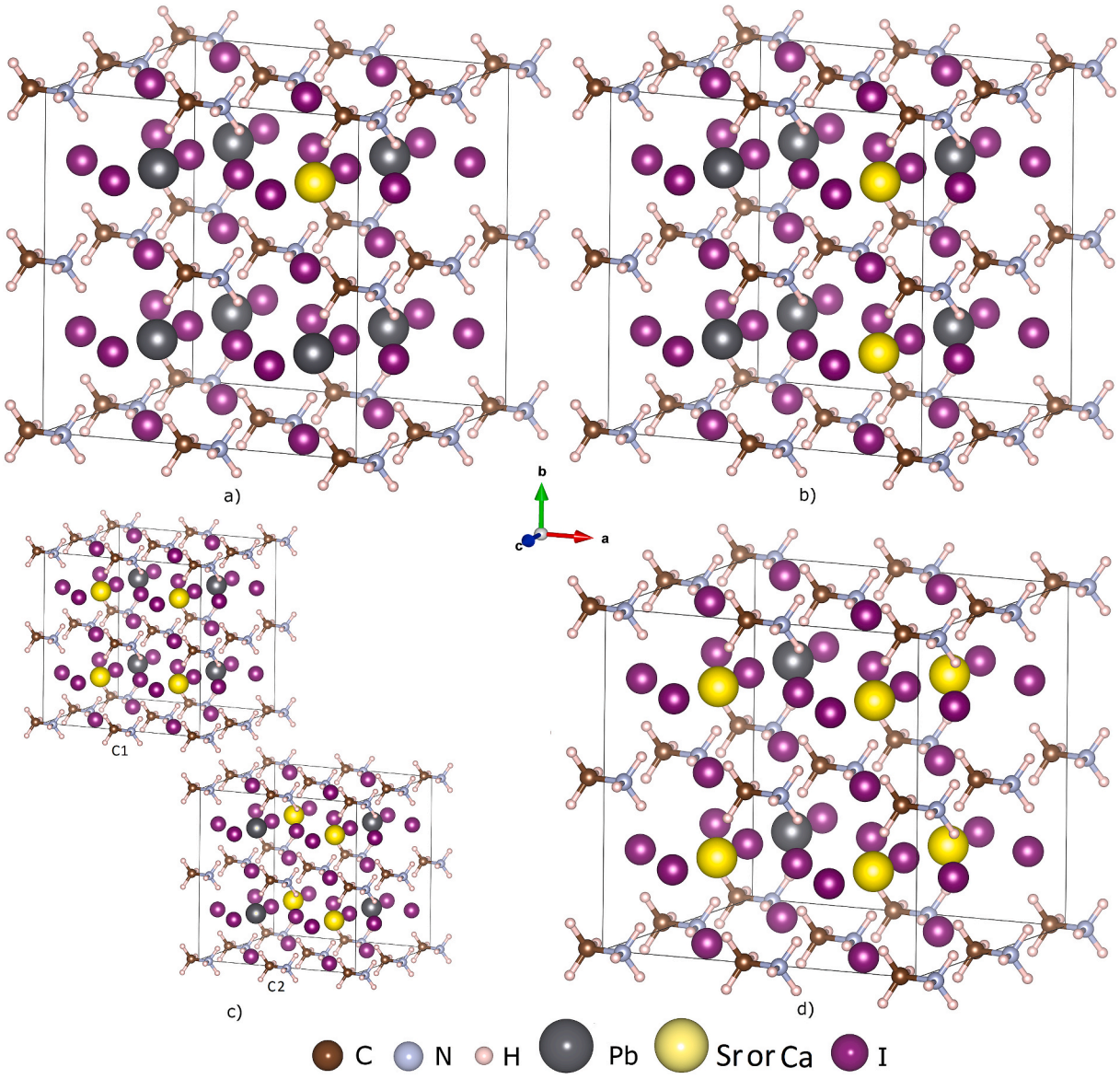

Fig. 2. The supercell crystal structures of $CH_3NH_3Pb_{(1-x)}Y_xI_3$ (Y=Sr, Ca) perovskite phases are designed by x ratio a) 0.125, b) 0.25, c) 0.50 (It is shown that the nearest neighbor substitutions in c1, the second nearest neighbor substitutions in c2), and d) 0.75, respectively. Brown, gray, cream, black, yellow, and purple circles in the pictures represent C, N, H, Pb, Sr or Ca and I atoms, respectively. (For interpretation of the references to colour in this figure legend, the reader is referred to the Web version of this article.)

Table 2
The calculated lattice constants of non-stoichiometric crystal structures of $CH_3NH_3Pb_{(1-x)}Y_xI_3$ (Y=Sr and Ca) perovskite phases are designed by x ratio a) 0.125, b) 0.25, c) 0.50 and d) 0.75, respectively.

Structure	x ratio	Lattice constants (A^0)			Angles between x, y, and z directions		
		a	*b*	*c*	*α*	*β*	*γ*
$CH_3NH_3Pb_{0.875}Sr_{0.125}I_3$	0.125	12.848	12.791	12.986	89.993	89.318	90.002
$CH_3NH_3Pb_{0.750}Sr_{0.250}I_3$	0.250	12.853	12.824	13.006	90.001	89.485	90.005
$CH_3NH_3Pb_{0.500}Sr_{0.500}I_3$	0.500	12.875	12.848	13.067	89.998	89.600	89.997
$CH_3NH_3Pb_{0.250}Sr_{0.750}I_3$	0.750	12.895	12.913	13.109	90.004	89.819	90.006
$CH_3NH_3Pb_{0.875}Ca_{0.125}I_3$	0.125	12.771	12.723	12.937	90.002	89.253	89.997
$CH_3NH_3Pb_{0.750}Ca_{0.250}I_3$	0.250	12.718	12.681	12.905	89.997	89.248	90.001
$CH_3NH_3Pb_{0.500}Ca_{0.500}I_3$	0.500	12.626	12.604	12.843	89.998	89.130	90.008
$CH_3NH_3Pb_{0.250}Ca_{0.750}I_3$	0.750	12.545	12.503	12.775	89.999	88.876	90.000

$CH_3NH_3SrI_3$ and $CH_3NH_3CaI_3$ structures are 3.261 eV ($Q\rightarrow\Gamma$ indirect) and 3.144 eV ($Q\rightarrow\Gamma$ indirect), respectively. Although the bandgaps of 3.261 eV and 3.144 eV are compatible with other theoretical studies [18, 19], they are very high for ideal photo absorbers.

Before explaining the causes of high bandgaps of $CH_3NH_3SrI_3$ and $CH_3NH_3CaI_3$ perovskite crystal structures by using electronegativity,

Table 3
The calculated band gaps of the stoichiometric $CH_3NH_3PbI_3$, $CH_3NH_3SrI_3$, and $CH_3NH_3CaI_3$ crystal structures and the other theoretical and experimental data.

Structure	Method	Band gap	Direction	Ref.
		$E_{bandgap}$ (eV)	Direct or Indirect	
$CH_3NH_3PbI_3$	our cal.	1.682	$R \rightarrow R$ Direct	
	other cal.	1.570	$\Gamma \rightarrow \Gamma$ Direct	[16]
		1.530	$\Gamma \rightarrow \Gamma$ Direct	[13]
		1.761		[14]
		1.540	$\Gamma \rightarrow \Gamma$ Direct	[15]
		1.420	$R \rightarrow R$ Direct	[17]
		1.600		[18]
		1.560	$R \rightarrow R$ Direct	[19]
		1.682	$R \rightarrow R$ Direct	[20]
		1.730	$R \rightarrow R$ Direct	[21]
		1.500	$R \rightarrow R$ Direct	[22]
		1.810	$R \rightarrow R$ Direct	[23]
		1.530		[26]
	exp.	1.550		[27]
		1.550		[28]
		1.610–1.680		[29]
		1.600	Direct	[30]
		1.550	Direct	[31]
$CH_3NH_3SrI_3$	our cal.	3.261	$Q \rightarrow \Gamma$ Indirect	
	other cal.	3.600		[18]
$CH_3NH_3CaI_3$	our cal.	3.144	$Q \rightarrow \Gamma$ Indirect	
	other cal.	3.400	$R \rightarrow \Gamma$ Indirect	[19]

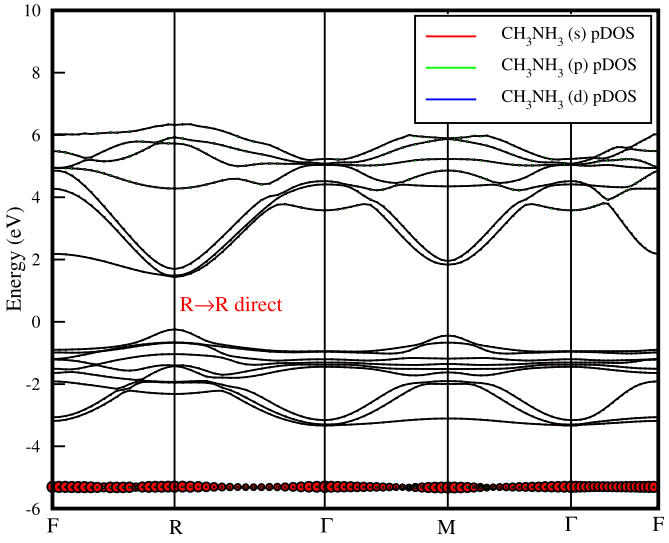

Fig. 3. The calculated pDOS for the organic $[CH_3NH_3]^+$ cation (A-type) part in the $CH_3NH_3PbI_3$ perovskite phase.

ionic radius, and antibonding characters, it is useful to give out which orbits the $[CH_3NH_3]^+$, Pb^{2+}, Sr^{2+}, Ca^{2+} cations and I^- anion contributes to the bandgap region. These data are presented in Figs. 3–7, respectively.

As can be seen in Fig. 3, in stoichiometric structures, there is little contribution to all regions of valence and conduction bands of $A-B-X_3$ phase from all of the s, p, and d orbits of the $[CH_3NH_3]^+$ cation. Therefore, the effect of cation $[CH_3NH_3]^+$ on the value of the bandgap is extremely small. However, there is a significant contribution from s orbit of $[CH_3NH_3]^+$ cation to around −5 eV.

Fig. 4 shows that the contributions from $Pb^{2+}p_x$ orbitals are spread over every region of the valence band. But is non-dominantly. However, there is a significant contribution from $Pb^{2+}p_x$ orbitals to the 3rd level

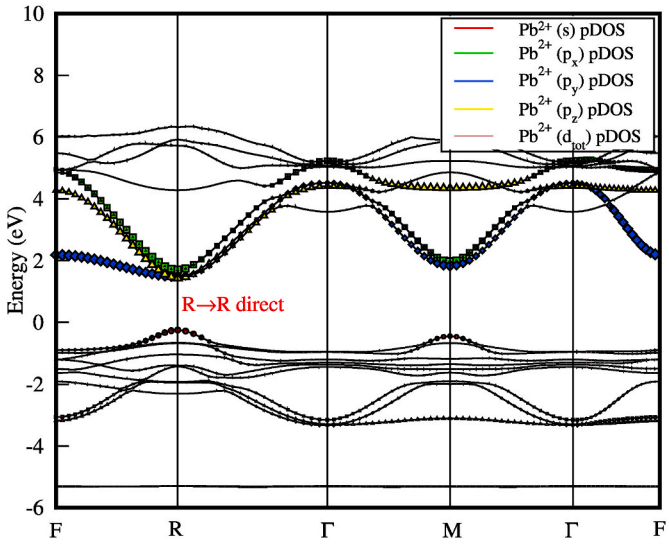

Fig. 4. The calculated pDOS for the Pb^{2+} cation (B type) part in the $CH_3NH_3PbI_3$ perovskite phase.

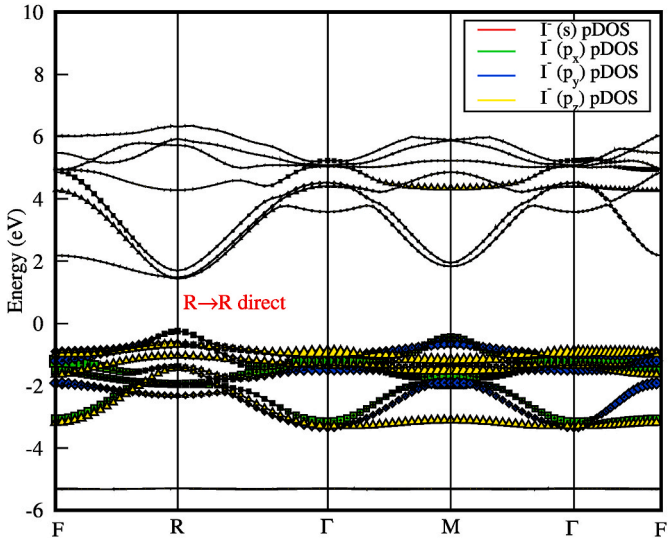

Fig. 5. The calculated pDOS for the I^- anion (X type) part in the $CH_3NH_3PbI_3$ perovskite phase.

energy region on the symmetry point R about approximately 1.69 eV at the lower levels of the conduction band. Moreover, the contributions from $Pb^{2+}p_y$ orbitals constitute the lowest conduction band. Therefore, it has a very impact on the value of the bandgap. Apart from this, it does not make a significant contribution to other regions. $Pb^{2+}p_z$ orbitals contribute to the lowest conduction band in the R symmetry point. Therefore, it can have a meaningful effect on the bandgap. It was observed that Pb^{2+} d orbitals did not have a significant contribution to the conduction and valence bands. As a result, $Pb^{2+}p_y$ and p_z orbitals will have an impact on the value of the bandgap of the material due to their significant contribution to the lowest conduction band.

Fig. 5 shows that although there is a significant contribution from I^- s orbitals to around −12 eV, no significant contribution is made to valence and conduction bands. Moreover, the I^- p_x orbitals make an intense contribution around −1.2 eV to −1.5 eV it is also very effective in forming the upper and lowest valence band. However, there is no significant contribution to the conduction band. I^-p_y orbitals play an important role in the formation of the middle region of the valence band.

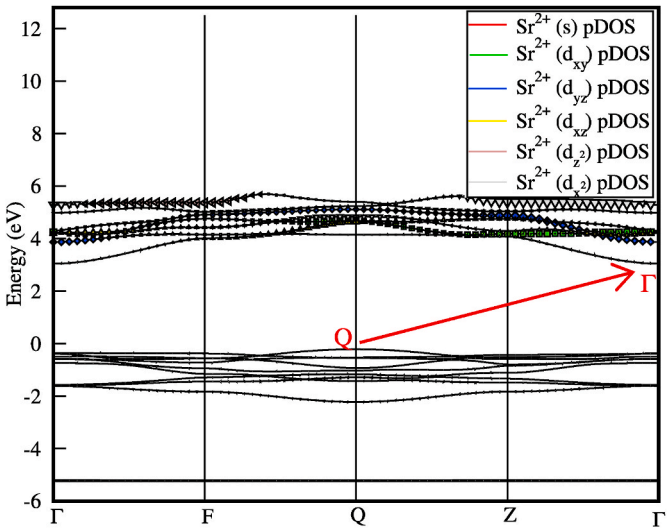

Fig. 6. The calculated pDOS for the Sr^{2+} cation (B type) part in the $CH_3NH_3SrI_3$ perovskite phase.

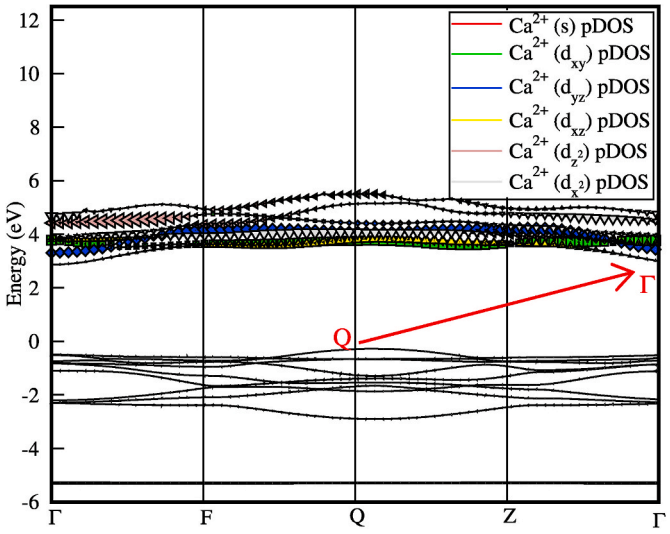

Fig. 7. The calculated pDOS for the Ca^{2+} cation (B type) part in the $CH_3NH_3CaI_3$ perovskite phase.

However, it is also effective in the upper valence band. Also, they contribute less than the contribution of the I^-p_x orbitals to the upper valance band. Besides, the character of the contributions from the I^-p_z orbitals to the valence bands are similar to the I^-p_y orbitals. There is also a small contribution to the 4.34 eV energy level of the conduction band of the I^-p_z orbitals. There is no significant contribution to valence and conduction bands from I^- d orbitals.

The effect of the Sr^{2+}substitution ion on the electronic structure is shown in Fig. 6. Firstly, an indirect band transition in the $Q\rightarrow\Gamma$ direction of the $CH_3NH_3SrI_3$ perovskite structure was calculated. There is no significant contribution from Sr^{2+} s orbitals. It contributes little to valence and conduction bands from Sr^{2+} p_x, p_y, and p_z orbitals. Moreover, there are minor contributions from the $Sr^{2+}d_{xy}$, d_{xz}, and d_{yz} orbitals to about 4.6 eV of the transmission band. Finally, there are contributions from Sr^{2+} d_{x^2} and d_{z^2} orbitals to the high levels of the conduction band (about 5.4 eV around).

The second substitution ion Ca^{2+}electronic behavior is presented in Fig. 7. It was determined that the band transition of the $CH_3NH_3CaI_3$ structure is in the direction of $Q\rightarrow\Gamma$ and indirectly. Ca^{2+} s, p_x, p_y, and p_z orbitals have no significant contribution to the valence bands. However, Ca^{2+} d_{xz} orbitals have little contribution to the valence band. Ca^{2+} d_{xy} orbitals contribute about 3.76 eV energy levels of the conduction band. Moreover, although they do not have direct contributions to the lowest point of the conduction band (Γ point), they will have relative effects on the bandgap as they contribute to the upper parts of the Γ point. Ca^{2+} d_{yz} orbitals support the medium energy levels of the conduction band. Finally, the Ca^{2+} d_{x^2} and d_{z^2} orbitals support the high levels of the conduction band. However, they have no significant contribution to valence bands.

According to the analysis given above, in terms of contributions from orbitals, the $[CH_3NH_3]^+$ cation has no dominant effect on the formation of bandgaps of stochiometric $CH_3NH_3PbI_3$, $CH_3NH_3SrI_3$, and $CH_3NH_3CaI_3$ structures. The Pb^{2+} a cation is very effective in the formation of the lowest conduction band. Moreover, the I^- anion is effective in the formation of the upper valence band. Therefore, the nature of Pb–I bonds significantly affects the value of the bandgap. When Pb–I bond energy changes with different ion substitution, the bandgap will increase or decrease depending on the electronegativity and ionic radius of the substitute ion.

As stated above, Firstly, the lowest parts of the *Pb* conduction band; *I*is dominant in the formation of the upper parts of the valence band as given Figs. 4 and 5.. Accordingly, the strength of ionic $Pb-I$ bonds is very effective in the formation of the bandgap. The strength of the ionic $Pb-I$ bonds results in a relatively smaller bandgap than $CH_3NH_3SrI_3$ (E_g = 3.261 eV), and $CH_3NH_3CaI_3$ (E_g = 3.144 eV), structures for $CH_3NH_3PbI_3$ (E_g = 1.682 eV) cubic perovskite structure. Secondly, The ionic radii of Pb^{2+} and Sr^{2+} ions are almost equal (about Sr^{2+} = 132 pm, Pb^{2+} = 133 pm). Therefore, cause the high bandgap of the $CH_3NH_3SrI_3$ structure, is not the inclusion of the Sr^{2+} ion in the crystal system. However, the electronegativity value of Sr is 0.95 and the electronegativity value of Pb is 2.33. When the $CH_3NH_3SrI_3$ structure is formed by substituting Sr^{2+} instead of Pb^{2+}ion, the electronegativity of the B cation in the crystal system decreases by 59.23%. Accordingly, since the $Sr-I$ antibonding character will increase, the bandgap of the $CH_3NH_3SrI_3$ structure will increase. As a result, the bandgap of the $CH_3NH_3SrI_3$ structure increased from 1.628 eV to 3.261 eV. If we focus on Ca^{2+} substitution, the ionic radius of the Ca ion is 114 pm, which is 14.29% smaller than the ionic radius of Pb. If the ionic radius is included in a smaller ion crystal system in the case of Ca^{2+} substitution for Pb^{2+}, the bandgap is expected to decrease. However, on the contrary, it was calculated that the bandgap of the $CH_3NH_3CaI_3$ structure increased. To explain this behavior, it is necessary to focus on the electronegativity of Ca and Pb. While Pb electronegativity is 2.33, Ca electronegativity is 1.00. When Ca^{2+} is substituted, the electronegativity of the B cation in the $CH_3NH_3CaI_3$ structure decreases by 57.08%. Accordingly, as the $Ca-I$ antibonding character increases, the value of the bandgap also increases (1.628 eV → 3.144 eV). This result shows that the effect of electronegativity change on the bandgap is more dominant than the effect of ionic radius difference.

3.4. Electronic properties of non-stoichiometric phases

It can be seen from the above calculations that the substitution ion exchanges such as $CH_3NH_3SrI_3$ and $CH_3NH_3CaI_3$ at stoichiometric ratios, are not sufficient applications for the perovskite $CH_3NH_3YI_3$ (Y═Sr, Ca) to have the ideal bandgap (about 1.5 eV according to SQ limit) for solar cells. Because $Pb-I$ bonds are extremely effective in the formation of the bandgap. For this reason, it is seen that to create a suitable mixture for the ideal bandgap, it is necessary to create compounds in non-stoichiometric ratios. Also, the Pb^{2+} concentration should be reduced as much as possible, but not completely removed, to reduce the toxic effect. Therefore, this part of the study focused on the electronic properties of non-stoichiometric $CH_3NH_3Pb_{(1-x)}Y_{(x)}I_3$ (Y═Sr, Ca, x = 0.125, 0.250, 0.500, and 0.75) compounds. Firstly, it was determined that the

band transitions were Γ→Γ direct in all non-stoichiometric $CH_3NH_3Pb_{(1-x)}Y_{(x)}I_3$ (Y=Sr, Ca, x = 0.125, 0.250, 0.500, 0.750) structures. The bandgaps of $CH_3NH_3Pb_{0.500}Sr_{0.500}I_3$ and $CH_3NH_3Pb_{0.250}Sr_{0.750}I_3$ phases were calculated as 1.796 eV and 1.964 eV, respectively. Similarly, the bandgaps in the $CH_3NH_3Pb_{0.500}Ca_{0.500}I_3$ and $CH_3NH_3Pb_{0.250}Ca_{0.750}I_3$ phases were also calculated as 1.739 eV and 1.936 eV, respectively. These values are high for ideal absorbers according to the SQ limit. Therefore, the details of these phases are not focused on. However, also the change in the electronic properties of the crystal in the case of Ca^{2+} and Sr^{2+} ions substituting in the second nearest neighbor positions for x = 0.50 has been studied. Substituting Ca^{2+} and Sr^{2+} ions at the diagonal cites as a second nearest neighbor for x = 0.50 have been changed the electronic structure of the material considerably. This change is higher than the electronic bandgaps (Γ→Γ direct) obtained for the nearest neighbor positions given in Table 4 by 17.67% for Ca^{2+} and 15.07% for Sr^{2+}.

At the second nearest neighbor for x = 0.50, it is not possible to explain this increase in electronic bandgaps by the change in concentration of Ca^{2+} or Sr^{2+} ions, electronegativity, and ionic radius change. We think that the most plausible way to explain the increase in the electronic bandgap due to the position change caused by the transfer of Ca^{2+} and Sr^{2+} ions from the nearest neighbor to the second-nearest neighbor for x = 0.50 is the increase of the antibonding effect between Pb–I and Ca–I bonds. Because the antibonding effect has one or more nodes in the bonding region between the nuclei. The density of the electrons in the orbital is concentrated outside the bonding region and acts to pull one nucleus away from the other and tends to cause mutual repulsion between the two atoms. For x = 0.50, when we take the Ca^{2+} and Sr^{2+} ions from its nearest neighbor to the second nearest neighbor position, we take both Pb^{2+} and Ca^{2+} or Sr^{2+} ions from the side part of the crystal to a diagonal position. This behavior pushes one core away from another. As the antibonding effect removes the cores from each other, the separation of the cores from each other can also increase the antibonding effect. Thus, indirectly increasing the antibonding effect on the Pb–I, Ca–I, and Sr–I bonds will cause an increase in the electronic bandgap. Because, from this situation, Pb–I, Ca–I, and Sr–I bonds will also be affected. However, when Ca^{2+} and Sr^{2+} ions are substituted at the diagonal cites as a second nearest neighbor position, the calculated electronic bandgaps (for Ca^{2+} 2.0462 eV and Sr^{2+} 2.0667 eV at x = 0.50) are not suitable for ideal photo absorbers. Therefore, this state, it was examined for testing purposes, its results discussed, but not given details.

However, as given Fig. 8, the bandgaps of $CH_3NH_3Pb_{0.875}Sr_{0.125}I_3$, $CH_3NH_3Pb_{0.750}Sr_{0.250}I_3$, $CH_3NH_3Pb_{0.875}Ca_{0.125}I_3$, and $CH_3NH_3Pb_{0.750}Ca_{0.250}I_3$ phases were calculated as 1.525 eV, 1.619 eV, 1.440 eV, and 1.540 eV, respectively. These are extremely suitable bandgaps for ideal photo absorbers. Also, the band transitions are Γ→Γ direct. This feature is more preferred for optoelectronic devices than indirect-transition semiconductors. As seen in Fig. 8, the contribution from I^- (X) anion in $CH_3NH_3Pb_{0.875}Sr_{0.125}I_3$, $CH_3NH_3Pb_{0.750}Sr_{0.250}I_3$, $CH_3NH_3Pb_{0.875}Ca_{0.125}I_3$ and $CH_3NH_3Pb_{0.750}Ca_{0.250}I_3$ compounds are dominant in the valence band (between −3.5 eV and 0 eV). Therefore, the I^- anion has a lot of influence on the stability of the $CH_3NH_3Pb_{(1-x)}Y_{(x)}I_3$ (Y=Sr, Ca) perovskite structure. The stability of the material is not negatively affected as the concentration of the I^- anion is kept constant in response to the changing Pb^{2+}, Sr^{2+}, and Ca^{2+} ions when substituting.

Table 4
The calculated band gaps of the non-stoichiometric $CH_3NH_3Pb_{(1-x)}Y_xI_3$ (Y=Sr and Ca) designed by the ratios of x = 0.125, 0.25, 0.50, and 0.75, respectively.

Structures	x ratio	Band gaps	Direction
		$E_{band-gap}$ (eV)	Direct or Indirect
$CH_3NH_3Pb_{0.875}Sr_{0.125}I_3$	0.125	1.525	Γ→Γ Direct
$CH_3NH_3Pb_{0.750}Sr_{0.250}I_3$	0.250	1.619	Γ→Γ Direct
$CH_3NH_3Pb_{0.500}Sr_{0.500}I_3$	0.500	1.796	Γ→Γ Direct
$CH_3NH_3Pb_{0.250}Sr_{0.750}I_3$	0.750	1.964	Γ→Γ Direct
$CH_3NH_3Pb_{0.875}Ca_{0.125}I_3$	0.125	1.440	Γ→Γ Direct
$CH_3NH_3Pb_{0.750}Ca_{0.250}I_3$	0.250	1.540	Γ→Γ Direct
$CH_3NH_3Pb_{0.500}Ca_{0.500}I_3$	0.500	1.739	Γ→Γ Direct
$CH_3NH_3Pb_{0.250}Ca_{0.750}I_3$	0.750	1.936	Γ→Γ Direct

The most important results of our study are four non-stoichiometric crystal compounds, which are given in Fig. 8 and whose bandgaps are around 1.5 eV, which is the ideal range according to the SQ limit. When comparing Sr^{2+} substitution given in Fig. 8a) and b) and Ca^{2+} substitution is given in Fig. 8c) and d), it was determined that the bandgap (1.44 eV and 1.54 eV, respectively) of the $CH_3NH_3Pb_{0.875}Ca_{0.125}I_3$ and $CH_3NH_3Pb_{0.750}Ca_{0.250}I_3$ compound formed as a result of the Ca^{2+} substitution is more suitable for ideal photo absorbers. Electronegativity decreased from 2.33 to 1.00 (approximately 57.08%) because Ca was substituted for Pb in the $CH_3NH_3CaI_3$ compound. It was also reduced by 14.29% in the ionic radius. Due to these changes, the bandgap of $CH_3NH_3CaI_3$ compounds increased from 1.68 eV to 3.144 eV. The reason for the increase of the bandgap is that the effect of electronegativity for Ca substitution is dominant compared to the effect of ionic radius reduction. However, Pb–I and Ca–I bonds to the electronic character of the $CH_3NH_3Pb_{0.875}Ca_{0.125}I_3$ and $CH_3NH_3Pb_{0.750}Ca_{0.250}I_3$ compounds have a common effect. With the screening effect of Pb–I interactions reduces the effect of a decrease in electronegativity by originated from Ca^{2+} substitution on the bandgap. With the effect of this behavior, the effect of ionic radius reduction becomes stronger, causing the bandgap of the material to decrease.

As given in Fig. 8 a), the bandgap has decrease although Sr^{2+} has been substituted in the $CH_3NH_3Pb_{0.875}Sr_{0.125}I_3$ and $CH_3NH_3Pb_{0.750}Sr_{0.250}I_3$ compounds. On the contrary, it was expected that the bandgap would grow as a result of the substitution of Sr^{2+} ion with lower electronegativity (0.95). The decrease in bandgap can be explained as follows. Although Sr electronegativity is smaller than Pb, the Pb concentration in the material is about 75% higher than the Sr concentration. Thus, the effect of Pb–I bonds is much stronger than Sr–I bonds. Consequently, the bandgap has not increased. Also, although the ionic radii are equal, the ionic radius of Sr^{2+} is about 0.75% smaller than Pb^{2+}. We think that this small decrease in the ionic radius reduces the bandgap from 1.682 eV to 1.525 eV. As seen in Fig. 8 b), as the Sr^{2+} concentration increases, the bandgap increases.

4. Conclusions

In this study, all non-stoichiometric substituted $CH_3NH_3Pb_{(1-x)}Y_{(x)}I_3$ (Y=Sr, Ca x = 0.125, 0.25, 0.50 and 0.75) crystal structures were calculated as a distorted orthorhombic phase as predicted by the tolerance factor range $0.7 < t < 0.9$. It is seen that the crystal structures of the non-stoichiometric phases are transformed from the cubic phase to a distorted orthorhombic phase, while the deviation rates in the lattice constants are very small.

The calculated bandgap (1.682 eV, R→R direct) is slightly high for an ideal photo absorber in the stoichiometric $CH_3NH_3PbI_3$ compound. Moreover, the bandgaps calculated for the stoichiometric $CH_3NH_3SrI_3$ and $CH_3NH_3CaI_3$ structures are 3.261 eV (Q→Γ indirect) and 3.144 eV (Q→Γ indirect), respectively. They are very high for ideal photo absorbers. Therefore, it is not possible to design a good solar cell material with Sr^{2+} and Ca^{2+} substitution at stoichiometric ratios. Because $Pb-I$ bonds are extremely effective in the formation of the bandgap and Pb^{2+} ions should not be completely removed from the crystal structure.

For this reason, it is focused that to create a suitable mixture form in non-stoichiometric ratios. Also, to reduce the toxic effect, the Pb^{2+} concentration was reduced as much as possible but not completely removed. Under these conditions, The bandgaps of the $CH_3NH_3Pb_{0.875}Sr_{0.125}I_3$, $CH_3NH_3Pb_{0.750}Sr_{0.250}I_3$, $CH_3NH_3Pb_{0.875}Ca_{0.125}I_3$, and $CH_3NH_3Pb_{0.750}Ca_{0.250}I_3$ phases were calculated as 1.525 eV, 1.619 eV, 1.440 eV, and 1.540 eV, respectively. These are extremely

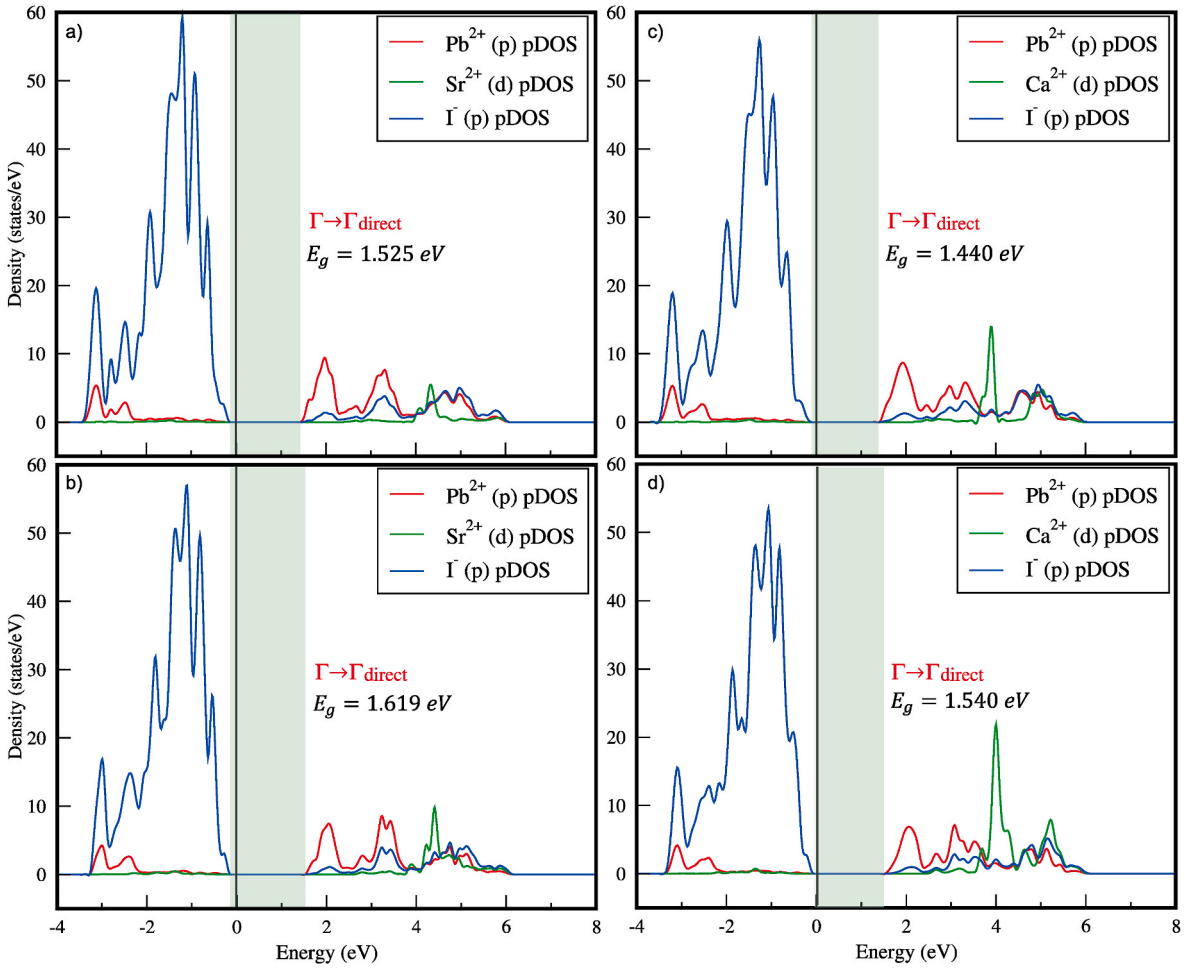

Fig. 8. Comparison of the phases studied in terms of ideal bandgaps. a) The calculated pDOS for the $CH_3NH_3Pb_{0.875}Sr_{0.125}I_3$ perovskite phase. b) The calculated pDOS for the $CH_3NH_3Pb_{0.750}Sr_{0.250}I_3$ perovskite phase. c) The calculated pDOS for the $CH_3NH_3Pb_{0.875}Ca_{0.125}I_3$ perovskite phase. d) The calculated pDOS for the $CH_3NH_3Pb_{0.750}Ca_{0.250}I_3$ perovskite phase. The vertical dot line represents the Fermi level shifted to 0 eV.

suitable bandgaps for ideal photo absorbers. Besides, the band transitions are Γ→Γ direct. This feature is more preferred for optoelectronic devices than indirect-transition semiconductors.

The most important results of our study are four non-stoichiometric crystal compounds, and whose bandgaps are around 1.5 eV, which is the ideal range according to the SQ limit. It was determined that the bandgap (1.44 eV and 1.54 eV, respectively) of the $CH_3NH_3Pb_{0.875}Ca_{0.125}I_3$ and $CH_3NH_3Pb_{0.750}Ca_{0.250}I_3$ compound formed as a result of the Ca^{2+} substitution is more suitable for ideal photo absorbers. Moreover, although the bandgaps of the $CH_3NH_3Pb_{0.875}Sr_{0.125}I_3$ (1.525 eV) and the $CH_3NH_3Pb_{0.750}Sr_{0.250}I_3$ (1.619 eV) phases is relatively higher than the Ca substitution, they have been found to have suitable bandgap for use in solar cell materials.

As a result, it was determined that the non-stoichiometric crystal structures in the form of the $CH_3NH_3Pb_{(1-x)}Ca_xI_3$ (x = 0.125, 0.250) obtained by Ca^{2+} substitution when compared to Sr^{2+} substitution are more suitable for their use in solar cells. One of the reasons is that the ionic radius of Ca^{2+} is 14.29% smaller than Pb^{2+}. The other is to allow a mixture of the effects of Pb–I and Ca–I bonds to determine the bandgap. On the contrary, because the electronegativity of Pb from Ca is 57.08% ratio small, it was determined that the bandgap was too high to be used in solar cells in cases of Ca substitution in $CH_3NH_3CaI_3$ compound.

CRediT authorship contribution statement

C. Soykan: Methodology, Software, Visualization, Writing - original draft, Writing - review & editing. **H. Gocmez:** Methodology, Supervision, Writing - review & editing.

Declaration of competing interest

The authors declare that they have no known competing financial interests or personal relationships that could have appeared to influence the work reported in this paper.

Acknowledgments

This work was supported by TUBITAK (The Scientific and Technological Research Council of Turkey) through project number 116F073. Computations are carried out on TUBITAK-ULAKBIM clusters. The authors would like to thank the institution and agency in carrying out this work. Finally, we would like to thank Dr. Sıtkı Eker for critical reading of this study.

References

[1] M. Gratzel, The light and shade of perovskite solar cells, Nat. Mater. 13 (2014) 838–842, https://doi.org/10.1038/nmat4065.
[2] J.M. Ball, M.M. Lee, A. Hey, H.J. Snaith, Low-temperature processed meso-superstructured to thin-film perovskite solar cells, Energy Environ. Sci. 6 (2013) 1739–1743, https://doi.org/10.1039/C3EE40810H.
[3] H.S. Kim, C.R. Lee, J.H. Im, K.B. Lee, T. Moehl, A. Marchioro, S.J. Moon, R. Humphry-Baker, J.H. Yum, J.E. Moser, M. Gratzel, Lead iodide perovskite sensitized all-solid-state submicron thin film mesoscopic solar cell with efficiency

exceeding 9% N, G. Park, Sci. Rep. 2 (2012) 591, https://doi.org/10.1038/srep00591.
[4] J. Burschka, N. Pellet, S.J. Moon, R. Humphry-Baker, P. Gao, M.K. Nazeeruddin, M. Gratzel, Sequential deposition as a route to high-performance perovskite-sensitized solar cells, Nature 499 (2013) 316–319, https://doi.org/10.1038/nature12340.
[5] J.H. Noh, S.H. Im, J.H. Heo, T.N. Mandal, S.I. Seok, Chemical management for colorful, efficient, and stable inorganic–organic hybrid nanostructured solar cells, Nano Lett. 13 (2013) 1764–1769, https://doi.org/10.1021/nl400349b.
[6] E. Mosconi, A. Amat, M.K. Nazeeruddin, M. Gratzel, FDe Angelis, First-principles modeling of mixed halide organometal perovskites for photovoltaic applications, J. Phys. Chem. C 117 (2013) 13902–13913, https://doi.org/10.1021/jp4048659.
[7] M.M. Lee, J. Teuscher, T. Miyasaka, T.N. Murakami, H.J. Snaith, Efficient hybrid solar cells based on meso-superstructured organometal halide perovskites Science. https://doi.org/10.1126/science.1228604, 2012, 338-643-647.
[8] M.Z. Liu, M.B. Johnston, H.J. Snaith, Efficient planar heterojunction perovskite solar cells by vapour deposition Nature. https://doi.org/10.1038/nature12509, 2013, 395-398.
[9] Y. Ogomi, A. Morita, S. Tsukamoto, T. Saitho, N. Fujikawa, Q. Shen, T. Toyoda, K. Yoshino, S.S. Pandey, T.L. Ma, S. Hayase, CH3NH3SnxPb(1-x)I3 perovskite solar cells covering up to 1060 nm, J. Phys. Chem. Lett. 5 (2014) 1004–1011, https://doi.org/10.1021/jz5002117.
[10] M. Graetzel, R.A.J. Janssen, D.B. Mitzi, E.H. Sargent, Materials interface engineering for solution-processed photovoltaics, Nature 488 (2012) 304–312, https://doi.org/10.1038/nature11476.
[11] P. Umari, E. Mosconi, FDe Angelis, Relativistic GW calculations on CH3NH3PbI3 and CH3NH3SnI3 perovskites for solar cell applications, Sci. Rep. 4 (2014) 4467, https://doi.org/10.1038/srep04467.
[12] F. Hao, C.C. Stoumpos, R.P.H. Chang, M.G. Kanatzidis, Anomalous band gap behavior in mixed Sn and Pb perovskites enables broadening of absorption spectrum in solar cells, J. Am. Chem. Soc. 136 (2014) 8094–8099, https://doi.org/10.1021/ja5033259.
[13] P.P. Sun, Q.S. Li, L.N. Yang, Z.S. Li, Theoretical insights into a potential lead-free hybrid perovskite: substituting Pb2+ with Ge2+, Nanoscale 8 (2016) 1503–1512, https://doi.org/10.1039/C5NR05337D.
[14] J. Chang, G. Wang, Y. Huang, X. Luo, H. Chen, New insights into the electronic structures and optical properties in the orthorhombic perovskite MAPbI3: a mixture of Pb and Ge/Sn, New J. Chem. 41 (2017) 11413–11421, https://doi.org/10.1039/C7NJ01442B.
[15] J. Navas, A. Sánchez-Coronilla, J.J. Gallardo, J.C. Piñero, D. De los Santos, E. I. Martín, N.C. Hernández, R. Alcántara, C. Fernández-Lorenzo, J. Martín-Calleja, The impact of Pd on the light harvesting in hybrid organic-inorganic perovskite for solar cells, Nanomater. Energy 34 (2017) 141–154, https://doi.org/10.1016/j.nanoen.2017.02.035.
[16] S. Chen, T. Bimenyimana, M. Guli, First-principles study on the electronic properties of perovskites $MASn_aPb_{(1-a)}X_bY_{(3-b)}$ (X, Y = Cl, Br, I) Results Phys 14 (2019) 102–408.
[17] Z.W. Xu, C.R. Zhang, Y.Z. Wu, J.J. Gong, W. Wang, Z.J. Liu, H.S. Chen, Density functional theory study on the electronic structures and related properties of Ag-doped $CH_3NH_3PbI_3$ perovskite, Results Phys 15 (2019) 102–709, https://doi.org/10.1016/j.rinp.2019.102709.
[18] T.J. Jacobsson, M. Pazoki, A. Hagfeldt, T. Edvinsson, Goldschmidt's rules and Strontium replacement in lead halogen perovskite solar cells: theory and preliminary experiments on $CH_3NH_3SrI_3$, J. Phys. Chem. C 119 (46) (2015) 25673–25683, https://doi.org/10.1021/acs.jpcc.5b06436.
[19] J.I. Uribe, D. Ramirez, J.M. Osorio, J. Osorio, F. Jaramillo, $CH_3NH_3CaI_3$ perovskite: synthesis, characterization, and first-principles studies, J. Phys. Chem. C 120 (30) (2016) 16393–16398, https://doi.org/10.1021/acs.jpcc.6b04207.
[20] C. Soykan, H. Goçmez, The physical properties of bismuth replacement in lead halogen perovskite solar cells: $CH_3NH_3Pb_{1-x}Bi_xI_3$ compounds by ab-initio calculations, Results Phys 13 (2019) 102–278, https://doi.org/10.1016/j.rinp.2019.102278.
[21] S. Rani, P. Singh, First principle study of electronic and optical properties of molecular ion (BF4-) substituted hybrid perovskite (CH3NH3PbI3), AIP Conf. Proc. 1832 (2017) 90035, https://doi.org/10.1063/1.4980588.
[22] M. Saffari, M.A. Mohebpour, H.R. Soleimani, M.B. Tagani, DFT analysis and FDTD simulation of CH3NH3PbI3-xClx mixed halide perovskite solar cells: role of halide mixing and light trapping technique, J. Phys. D Appl. Phys. 50 (2017) 415–501, https://doi.org/10.1088/1361-6463/aa83c8.
[23] S.X. Tao, X. Cao, P.A. Bobbert, Accurate and efficient bandgap predictions of metal halide perovskites using the DFT-1/2 method, GW accuracy with DFT expense. Sci. Rep 7 (2017) 14386, https://doi.org/10.1038/s41598-017-14435-4.
[24] A. Poglitsch, D. Weber, Dynamic disorder in methylammoniumtrihalogenoplumbates (II) observed by millimeter-wave spectroscopy, J. Chem. Phys. 87 (637) (1987) 3–8, https://doi.org/10.1063/1.453467.
[25] Y. Ando, T. Oku, Y. Ohishi, Rietveld refinement of the crystal structure of perovskite CH3NH3(Sb)I3 solar cells, Japan, J. Appl. Phys. 57 (2018), 02CE02, https://doi.org/10.7567/JJAP5702CE02.
[26] E. Mosconi, B. Merabet, D. Meggiolaro, A. Zaoui, F.D. Angelis, First-principles modeling of bismuth doping in the MAPbI3 perovskite, J. Phys. Chem. C 122 (2018), https://doi.org/10.1021/acs.jpcc.8b01307, 14107–12.
[27] A. Kojima, K. Teshima, Y. Shirai, T. Miyasaka, Organometal halide perovskites as visible-light sensitizers for photovoltaic cells, J. Am. Chem. Soc. 131 (2009) 6050, https://doi.org/10.1021/ja809598r. –1.
[28] Y. Dang, X. Tao, Y. Liu, Y. Sun, D. Yuan, X. Liu, et al., Bulk crystal growth of hybrid perovskite material CH3NH3PbI3, RSC Pub. Cryst. Eng. Comm. (2013) 1–3, https://doi.org/10.1039/C4CE02106A, 00.
[29] J.Q. Phuong, Y. Yamada, M. Nagai, N. Maruyama, A. Wakamiya, Y. Kanemitsu, Free carriers versus excitons in CH3NH3PbI3 perovskite thin films at low temperatures: charge transfer from the orthorhombic phase to the tetragonal phase, J. Phys. Chem. Lett. 7 (2016) 13–23, https://doi.org/10.1021/acs.jpclett.6b00781, 16–21.
[30] Y. Yamada, T. Nakamura, M. Endo, A. Wakamiya, Y. Kanemitsu, Near-band-edge optical responses of solution-processed organic-inorganic hybrid perovskite CH3NH3PbI3 on mesoporous TiO2 electrodes, APEX 7 (2014) 32302, https://doi.org/10.7567/APEX.7.032302.
[31] H.S. Kim, C.R. Lee, J.H. Im, K.B. Lee, T. Moehl, A. Marchioro, et al., Lead iodide perovskite sensitized all-solid-state submicron thin film mesoscopic solar cell with efficiency exceeding 9%, Sci. Rep. 2 (2012) 591, https://doi.org/10.1038/srep00591.
[32] W. Shockley, H.J. Queisser, Detailed balance limit of efficiency of p-n Junction Solar Cells, J. Appl. Phys. 32 (1961) 510, https://doi.org/10.1063/1.1736034.
[33] P. Hohenberg, W. Kohn, Inhomogeneous electron gas, Phys. Rev. B 136 (1964) 864, https://doi.org/10.1103/PhysRev.136.B864.
[34] W. Kohn, L.J. Sham, Self-consistent equations including exchange and correlation effects, Phys. Rev. 140 (1965) 1133, https://doi.org/10.1103/PhysRev.140.A1133.
[35] W. Kohn, A.D. Becke, R.G. Parr, Density functional theory of electronic structure, J. Phys. Chem. 100 (1996) 974, https://doi.org/10.1021/jp9606691.
[36] G. Kresse, J. Furthmuller, Efficiency of ab-initio total-energy calculations for metals and semiconductors using a plane-wave basis set, Comput. Mater. Sci. 6 (1996) 15–50, https://doi.org/10.1016/0927-0256(96)00008-0.
[37] G. Kresse, J. Furthmuller, Efficient iterative schemes for ab-initio total-energy calculations using a plane-wave basis set, Phys. Rev. B 54 (1996) 11169, https://doi.org/10.1103/PhysRevB.54.11169.
[38] J. Hafner, Materials simulations using VASP a quantum perspective to materials science, Comput. Phys. Commun. 177 (2007) 6–13, https://doi.org/10.1016/j.cpc.2007.02.045.
[39] G. Kresse, J. Hafner, Ab initio molecular dynamics for liguid metals, Phys. Rev. B 47 (1993) 558, https://doi.org/10.1103/PhysRevB.47.558.
[40] G. Kresse, J. Hafner, Norm-conserving and ultrasokf pseudopotentials for first-row and transition elements, J. Phys. Condens. Matter 6 (1994) 8245, https://doi.org/10.1088/0953-8984/6/40/015.
[41] J.P. Perdew, K. Burke, M. Ernzerhof, Generalized gradient approximation made simple, Phys. Rev. Lett. 77 (1996) 3865, https://doi.org/10.1103/PhysRevLett.77.3865.
[42] P.E. Blöchl, Projector augmented-wave method, Phys. Rev. B 50 (1994) 17953–17978, https://doi.org/10.1103/PhysRevB.50.17953.
[43] H.J. Monkhorst, J.D. Pack, Special points for Brillouin-zone integrations, Phys. Rev. B 13 (1976) 5188–5192, https://doi.org/10.1103/PhysRevB.13.5188.
[44] V.M. Goldschmidt, Die gesetze der Krystallochemie, Naturwissenschaften 14 (1926) 477–485, https://doi.org/10.1007/BF01507527.
[45] J. Calabrese, N.L. Jones, R.L. Harlow, N. Herron, D.L. Thorn, Y. Wang, Preparation and characterization of layered lead halide compounds, J. American Chem. Soc. 113 (1991) 2328–2330, https://doi.org/10.1021/ja00006a076.
[46] D.B. Mitzi, S. Wang, C.A. Feild, C.A. Chess, A.M. Guloy, Conducting layered organic-inorganic halides containing <110>-Oriented perovskite sheets, Sci 267 (1995) 1473–1476, https://doi.org/10.1126/science.267.5203.1473.
[47] H.G. Kim, O.S. Becker, J.S. Jang, S.M. Ji, P.H. Borse, S.J. Lee, A generic method of visible light sensitization for perovskite-related layered oxides: substitution effect of lead, J. Solid State Chem. 179 (2006) 1214–1218, https://doi.org/10.1016/j.jssc.2006.01.024.
[48] F. Wang, I. Grinberg, A.M. Rappe, Bandgap engineering strategy via polarization rotation in perovskite ferroelectrics, Phys. Lett. 104 (2014) 1–4, https://doi.org/10.1063/1.4871707, 152903.
[49] C. Grote, B. Ehrlich, R.F. Berger, Tuning the near-gap electronic structure of tin-halide and lead-halide perovskite via changes in atomic layering, Phys. Rev. B 90 (2014) 1–7, https://doi.org/10.1103/PhysRevB.90.205202, 205202.